A&A 633, L6 (2020)
https://doi.org/10.1051/0004-6361/201937144

Astronomy & Astrophysics

LETTER TO THE EDITOR

First direct observation of a torsional Alfvén oscillation at coronal heights*

P. Kohutova[1,2], E. Verwichte[3], and C. Froment[1,2,4]

[1] Rosseland Centre for Solar Physics, University of Oslo, PO Box 1029, Blindern 0315, Oslo, Norway
e-mail: petra.kohutova@astro.uio.no
[2] Institute of Theoretical Astrophysics, University of Oslo, PO Box 1029, Blindern 0315, Oslo, Norway
[3] Centre for Fusion, Space and Astrophysics, Department of Physics, University of Warwick, Coventry CV4 7AL, UK
[4] LPC2E, CNRS and University of Orléans, 3A avenue de la Recherche Scientifique, Orléans, France

Received 19 November 2019 / Accepted 7 December 2019

ABSTRACT

Context. Torsional Alfvén waves are promising candidates for the transport of energy across different layers of the solar atmosphere. They have been predicted theoretically for decades. Previous detections of Alfvén waves so far have however mostly relied on indirect signatures.
Aims. We present the first direct observational evidence of a fully resolved torsional Alfvén oscillation of a large-scale structure occurring at coronal heights.
Methods. We analysed IRIS imaging and spectral observation of a surge resulting from magnetic reconnection between active region prominence threads and surrounding magnetic field lines.
Results. The IRIS spectral data provide clear evidence of an oscillation in the line-of-sight velocity with a 180° phase difference between the oscillation signatures at opposite edges of the surge flux tube. This together with an alternating tilt in the Si IV and Mg II k spectra across the flux tube and the trajectories traced by the individual threads of the surge material provide clear evidence of torsional oscillation of the flux tube.
Conclusions. Our observation shows that magnetic reconnection leads to the generation of large-scale torsional Alfvén waves.

Key words. magnetohydrodynamics (MHD) – Sun: corona – Sun: oscillations – Sun: magnetic fields

1. Introduction

The magnetised solar atmosphere supports a variety of magnetohydrodynamic (MHD) waves (Nakariakov & Verwichte 2005). In homogeneous plasma, such waves are either magnetoacoustic or purely magnetic. It should be noted that this distinction is only clear in specific geometries because in realistic non-homogeneous plasma the different MHD modes are coupled and can have mixed properties (e.g. Goossens et al. 2012). The magnetic, or Alfvén waves, are incompressible and dispersionless. Alfvén waves are difficult to dissipate in the absence of large gradients in local Alfvén speed. They are therefore prime candidates for being responsible for transfer of energy between different layers of solar atmosphere.

In the case of an ideal magnetic flux tube, which is a valid approximation for most magnetic structures observed in the solar atmosphere, the incompressible Alfvén mode corresponds to a torsional wave characterised by perturbations in the azimuthal components of velocity and magnetic field corresponding to a periodic axisymmetric rotation (Edwin & Roberts 1983). A torsional Alfvén wave excited along a coronal flux tube does not perturb the density of the flux tube and therefore does not modify the emission. Because of this, the torsional Alfvén modes are notoriously difficult to observe. Their main observational signature is that of opposite and alternating Doppler shifts at opposite edges of the flux tube (Van Doorsselaere et al. 2008). In practice, this corresponds to an alternating spectral line tilt seen in spectra taken across the oscillating structure.

Previous reports of Alfvén mode detection have so far mostly relied on indirect signatures, such as periodic broadening of spectral line width resulting from unresolved opposite Doppler shifts across the structure. Similar oscillations in the full width at half maximum (FWHM) of the Hα spectral line across magnetic bright point were reported by Jess et al. (2009). Observations of opposite Doppler shifts in chromospheric spicules that are spatially resolved have been reported by Srivastava et al. (2017), although these observations show only isolated cases of Doppler shift reversal and therefore lack evidence of the oscillatory behaviour. Direct observational evidence of the torsional Alfvén mode in the solar atmosphere that is both spatially and temporally resolved is still missing.

Reports of uni-directional twisting motions are much more prevalent. Such motion has been observed in spicules (De Pontieu et al. 2012), swirls, and tornados (Wedemeyer-Böhm et al. 2012; Shetye et al. 2019). It has also been observed during eruptive events consisting of ejection of solar plasma from the lower solar atmosphere into the corona as a result of magnetic reconnection, most notably in jets and surges (e.g. Schmieder et al. 2013; Filippov et al. 2015; Xue et al. 2016). In that case, rotation is interpreted as an untwisting of the magnetic flux rope involved in the eruption

* Movies attached to Figs. 1 and 2 are available at https://www.aanda.org

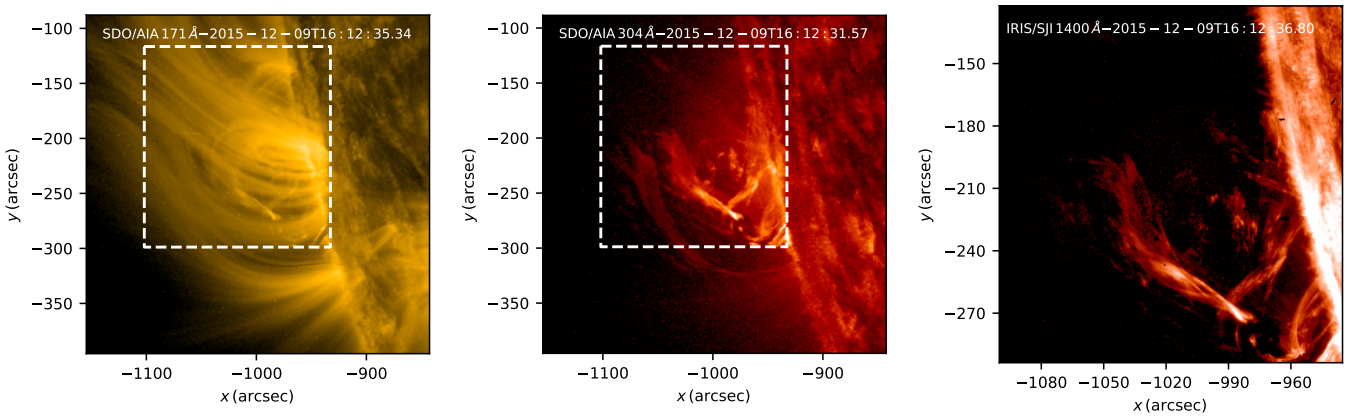

Fig. 1. Snapshots of the studied active region immediately following the surge eruption as observed at 16:12:35 in AIA 171 Å (*left*), AIA 304 Å (*middle*), and IRIS SJI 1400 Å (*right*). The dashed line in the AIA images outlines the IRIS field of view. Animation of this figure is available online.

(Iijima & Yokoyama 2017). The release of magnetic twist accumulated in the flux rope involved in the magnetic reconnection can result in overshooting the equilibrium of the newly formed flux tube and in the excitation of a torsional oscillation propagating at Alfvén speed. The mechanism of torsional wave generation by relaxation of twisted magnetic field has been proposed from theoretical models (Shibata & Uchida 1986; Velli & Liewer 1999; Pariat et al. 2009; Török et al. 2009), but has not yet been observed.

2. Observation

We analysed an event from 9 December 2015 occurring in NOAA AR 12468 observed by the Interface Region Spectrograph (IRIS; De Pontieu et al. 2014a). The IRIS level 2 slit-jaw imager (SJI) and spectrograph (SG) data used for analysis were taken between 16:12 and 17:11 UT. The SJI data were taken in two passbands; the far-ultraviolet (FUV) and the near-ultraviolet (NUV). The FUV passband is centred on 1400 Å and is dominated by two Si IV lines formed at $\log T = 4.8$ in the transition region; the NUV passband is centred on 2796 Å dominated by the Mg II K line core formed at $\log T = 4$ in the chromosphere. The SJI data have an exposure time of 8 s, 19 s cadence, and an image scale of 0.166″ pixel^{-1}. The IRIS observations were taken in sit-and-stare mode with a field of view of 167″ × 174″ centred at $x, y = [-1017'', -209'']$. The SG slit is fixed at $x = 1017''$.

We further used imaging EUV data from the Atmospheric Imaging Assembly (AIA) on board the Solar Dynamics Observatory (SDO) (Lemen et al. 2012) in 171 Å and 304 Å passbands providing context images for plasma at coronal and transition region temperatures respectively. Level 1.5 SDO/AIA data have the image scale of 0.6″ pixel^{-1}, 12 s cadence and were normalised by the exposure time.

We focus on the NOAA AR 12468 active region at the eastern limb (Fig. 1). Prominence with twisted flux-rope structure spanning across the whole active region can be observed at the limb in AIA 304 Å and in the IRIS FUV and NUV SJI channels. The active region also contains footpoints of coronal loops with radii of the order of 100 Mm as well as several open magnetic field lines. Magnetic reconnection involving several prominence threads occurs in the foreground component of the prominence at 16:02 UT, when they can be observed to erupt and reconnect with surrounding open and closed magnetic field lines. The reconnection event is accompanied by a surge of cool plasma previously confined in the prominence flux rope. As the IRIS observing sequence starts at 16:12:36 UT, the analysis of the reconnection event itself is limited to imaging data from SDO/AIA.

This IRIS dataset has previously been analysed by Kohutova et al. (2019) and Schad (2018) with a focus on coronal rain. In particular, Kohutova et al. (2019) perform a detailed analysis of the reconnection event, the onset of thermal instability and associated coronal rain formation in one of the coronal loops. The analysis therein however excludes the upward-moving surge material and the associated downflows. In this study we focus on the evolution of the surge and the associated oscillatory motion following the reconnection.

3. Torsional surge oscillation

The reconnection of the individual prominence threads with surrounding coronal structures leads to a fraction of the cool prominence plasma being ejected away from the reconnection region. The bulk of the ejected material consists of two main components denoted as S1 and S2 in Fig. 2. Component S1 moves upwards freely and undergoes helical motion believed to be the result of the reconnection of a twisted bundle of prominence threads with overlying field lines. Helical motion of the ejected surge material suggests that the reconnection lead to the release of the magnetic twist accumulated in the flux rope supporting the prominence. The ejection of component S2 is triggered by the reconnection of a prominence thread with a closed coronal loop. The confined material then moves along a closed loop-like trajectory and subsequently falls towards the solar surface.

The direction of the helical motion of the surge material alternates, suggesting a large-scale torsional wave is set up in the flux tube following the reconnection. The helical motion of the individual threads is observable both in the imaging and spectral data. Rotation in a clockwise direction viewed edge-on is revealed in spectral data as opposite red and blue-shifted emission on the top and bottom edges of the flux tube, relative to the mean line-of-sight velocity. The reverse is true for a counter-clockwise rotation. The IRIS SG slit is in sit-and-stare mode and crosses the surge material at an angle. As a result, it is possible to determine the presence and direction of rotation from variations of the Doppler shift as a function of distance along the slit. Figure 2 shows SJI snapshots at various phases of the torsional motion of the flux tube as well as the Si IV and Mg II K line profiles along the slit between $y = -254''$ and $y = -244''$,

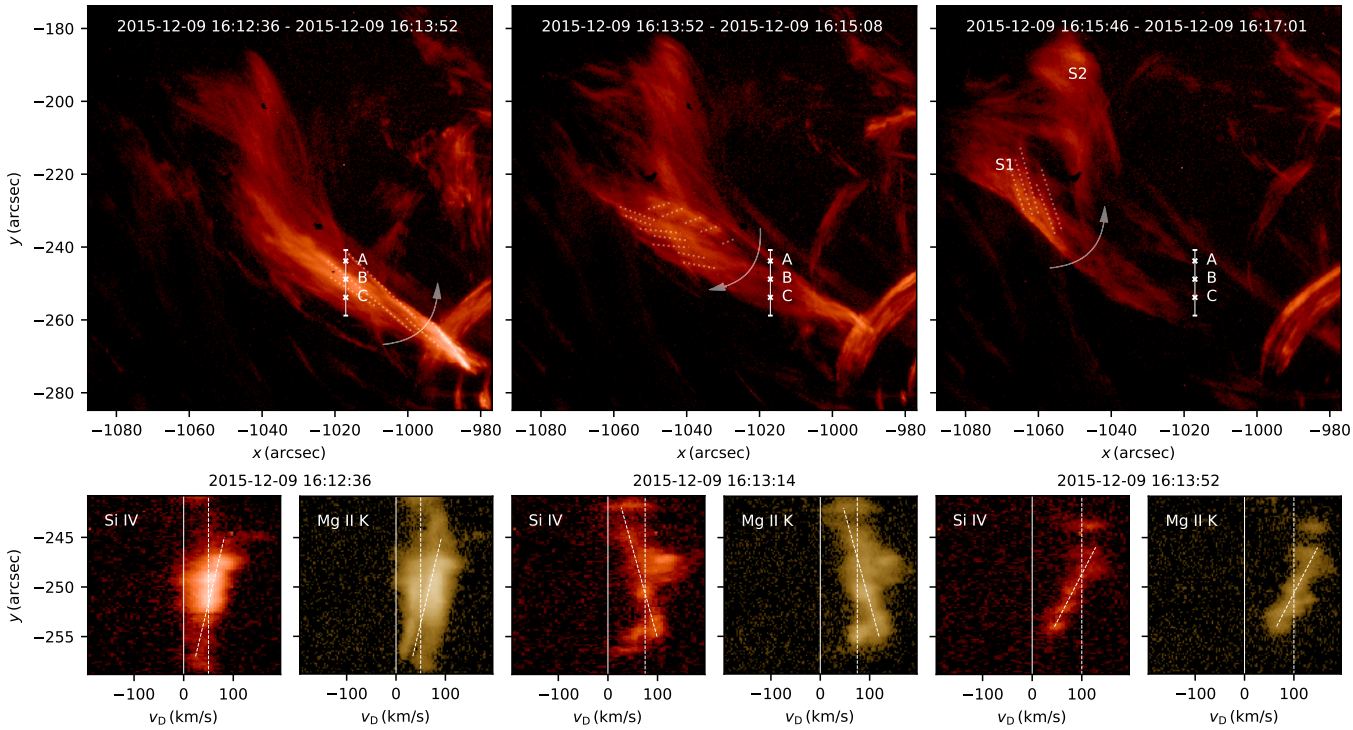

Fig. 2. Evolution of the rotating flux tube. *Top*: superimposed snapshots in IRIS FUV SJI data during three different phases of the torsional oscillation of the surge material. White dotted lines outline the helical trajectories of the plasma threads. The arrow shows the direction of the rotation. The white vertical line corresponds to the fraction of the slit intersecting the surge plasma. The freely moving and confined component of the ejected surge material are denoted S1 and S2, respectively. *Bottom*: IRIS Si IV and Mg II K spectra of the surge material corresponding to the fraction of the slit marked by the white line. We show spectral snapshots from three different phases of the motion of the plasma at the slit position. In each panel, the vertical dashed line indicates the mean Doppler velocity of the plasma. The alternating tilt of the emission in the different phases, denoted in each panel by the tilted dashed line (obtained by visual examination) corresponds to the torsional motion of the surge material. Animation of this figure is available online.

where the slit intersects with the surge material. We note that the imaging and spectral snapshots are not concurrent because by the time the third phase of the propagating oscillation is visible in the upper part of the flux tube, there is no observable emission at the slit position. The mean Doppler velocity detected in the surge material is positive and increases with time from $\sim$50 km s^{-1} to over 100 km s^{-1} when the bulk of the surge material passes the SG slit. Immediately following the reconnection event the torsional motion in a counter-clockwise direction is first detected. The centres of both Si IV and Mg II K line profiles show positive gradients with respect to distance along the slit, i.e. $\mathrm{d}v_\mathrm{D}/\mathrm{d}y > 0$. Approximately 40 s later, the direction of rotation reverses and $\mathrm{d}v_\mathrm{D}/\mathrm{d}y < 0$. Finally, during the last phase when the surge material remains visible in the spectral data the sense of rotation reverses once more and the line profile gradient becomes positive again. During all three time intervals, the position of the line centres is not a perfectly monotonic function of y. This suggests the presence of further small-scale motions within the flux tube in addition to the large-scale torsional motion.

Both Si IV and Mg II K line profiles are fitted with a single peak Gaussian because the central reversal in the Mg II K line core is not present in most of the features observed off-limb. Figure 3 shows the evolution of the line profile parameters at three locations along the SG slit, indicated by A, B, and C in Fig. 2, for a time interval of 180 s when the surge material is observable in the spectral data. Locations A and C correspond to the two edges of the flux tube and B corresponds to the centre of the flux tube. The peak Si IV and Mg II K line intensities gradually decrease with time as the bulk of the surge material passes the slit, with the exception of the top edge of the flux tube near location A, where the surge plasma is more sparse. The torsional oscillation is clearly visible in the temporal evolution of the Doppler velocity as an anti-phase oscillation at the opposite edges of the flux tube. The Si IV and Mg II K spectral line widths first rapidly increase, which is then followed by more gradual decrease. This suggests that the plasma is gradually cooling except for a short period of impulsive heating immediately after the reconnection event. The evolution of all three profile parameters becomes less clear after the initial 150 s of the IRIS observing sequence; this is because most of the surge material has by then moved past the slit and is only visible in the upper part of the IRIS SJI field of view.

The Doppler velocity oscillation at opposite edges of the flux tube (locations A and C) is obtained from the Si IV spectra by removing the linear trend from the Doppler velocity time series. The linear trend is due to the line-of-sight component of the surge bulk motion. We fit a damped sine function of the form $\delta v_\mathrm{D}(t) = v_0 \exp(-t/\tau)\sin(\frac{2\pi t}{P} + \phi_\mathrm{A,C})$. The amplitude v_0, period P, damping scaling time τ, and phase ϕ are free parameters fitted using weighted least squares to both A and C time series simultaneously subject to the constraint that $\phi_\mathrm{A} - \phi_\mathrm{C} = \pi$. The weights are the inverse of the mean relative residuals of the individual Gaussian line profile fits at each time step, which are a measure of goodness-of-fit of a simple Gaussian function for the line profile. We find $v_0 = 41$ km s^{-1}, $P = 89$ s, and $\tau = 136$ s. It should be noted that the phase difference between the two time series is expected to be slightly less than as 180° as the SG slit is not perpendicular to the flux tube axis but intersects it at an angle.

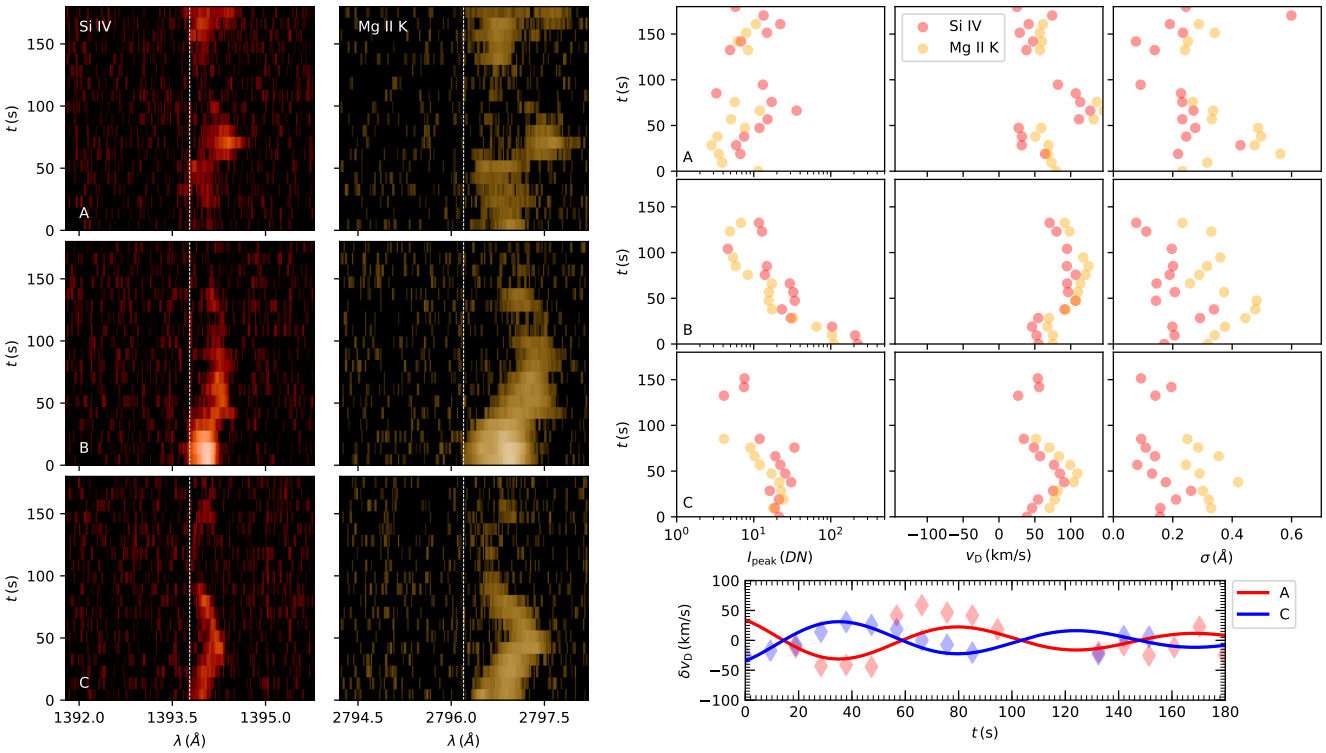

Fig. 3. *Left*: evolution of Si IV and Mg II K line profiles during the initial surge phase at the three points A, B, and C shown in Fig. 2 corresponding to the top edge of the surge, surge centre, and bottom edge of the surge, respectively. *Left*: wavelength-time plot for Si IV (red) and Mg II K (orange) spectra during the initial 180 s when the surge material is detectable in the SG data, starting at 16:12:36. *Top right*: evolution of the parameters of the line profiles fitted with a single peak Gaussian. The scatter plots correspond to the peak intensity, Doppler velocity, and line width at points A, B, and C. We omit instances in which the profiles could not be fitted reliably. *Bottom right*: evolution of the line-of-sight velocities at the opposite edges of the flux tube fitted to detrended Si IV spectra.

As the torsional oscillation is propagating, we do not measure at a fixed time the same phase of the oscillation in both locations.

We estimate the speed of the torsional wave propagation to be 170 km s^{-1} in the plane of the sky using time-distance plots along the axis of the surge flux tube. Assuming the angle between the surge propagation and the line of sight to be 45°, the speed of the bulk plasma flow in the plane of the sky is the same as the speed along the line of sight, which we estimate to be 70 km s^{-1} from the mean Doppler shift. This leads to the projected net phase speed of the oscillation of 100 km s^{-1} in the plane of the sky resulting in the total phase speed of 140 km s^{-1}. This is consistent with expected Alfvén speed of ∼180 km s^{-1} in a comparable structure given by $v_A = B/\sqrt{\mu_0 \rho}$, assuming the plasma density of prominence material of 10^{-10} kg m^{-3} and a magnetic field strength of 20 G, i.e. typical values for prominences (e.g. Mackay et al. 2010).

4. Discussion and conclusions

The observed anti-phase oscillations of Doppler velocity perturbations are subject to attenuation with a typical scaling time measured to be 136 s. Torsional oscillations occurring in a non-homogeneous plasma dissipate their energy via phase mixing (Luo et al. 2002; Soler et al. 2019). Phase mixing is caused by variations in the plasma quantities in a direction perpendicular to the magnetic field leading to variations in the local Alfvén speed (Heyvaerts & Priest 1983). This results in Alfvén waves on different magnetic surfaces propagating with different speeds and becoming increasingly out of phase, thereby leading to enhanced dissipation. However, for this mechanism to be observed, it would be necessary to track the wave amplitude of the propagating wave, which is not possible in a fixed-slit observation. Instead, we measure the amplitude profile of the torsional wave train.

Accumulation of magnetic twist is common both in the lower solar atmosphere in the form of small-scale twisted magnetic elements (De Pontieu et al. 2014b) and at coronal heights in prominence flux ropes (Mackay et al. 2010). The mechanism of reconnection-induced twist release and associated generation of torsional oscillations is easier to resolve in large-scale structures, however, the occurrence of such a process can be expected to be ubiquitous on smaller scales. The magnetic twist originates from twisting and braiding of the footpoints of magnetic structures from magnetoconvective vortex flows (Shelyag et al. 2011), or from magnetic flux ropes emerging from the solar interior into the solar atmosphere (Archontis 2012). Magnetic reconnection is one of the physical processes responsible for the transfer of magnetic helicity from the lower solar atmosphere into the corona.

We present the first spatially and temporally resolved observation of a torsional Alfvén wave in a large-scale structure at coronal heights, detecting clear anti-phase oscillation of line-of-sight velocities at the opposite edges of the flux tube. We have shown that the magnetic reconnection leads to the generation of torsional Alfvén waves. This suggests that the omnipresent small-scale reconnection events occurring in the lowermost layers of the solar atmosphere involving twisted magnetic elements are capable of Alfvén wave excitation on global scales.

Acknowledgements. This research was supported by the Research Council of Norway through its Centres of Excellence scheme, project no. 262622.

E.V. acknowledges financial support from the UK STFC on the Warwick STFC Consolidated Grant ST/L000733/I. C.F. acknowledges funding from CNES. The SDO/AIA data are available courtesy of NASA/SDO and the AIA science team. 1.5 SDO/AIA data are available from AIA cutout service web page http://www.lmsal.com/get_aia_data/. IRIS is a NASA small explorer mission developed and operated by LMSAL with mission operations executed at NASA Ames Research center and major contributions to downlink communications funded by the Norwegian Space Center (NSC, Norway) through an ESA PRODEX contract. IRIS data are available from mission web page http://iris.lmsal.com/search.

References

Archontis, V. 2012, Phil. Trans. R. Soc. A, 370, 3088
De Pontieu, B., Carlsson, M., Rouppe van der Voort, L. H. M., et al. 2012, ApJ, 752, L12
De Pontieu, B., Title, A. M., Lemen, J. R., et al. 2014a, Sol. Phys., 289, 2733
De Pontieu, B., Rouppe van der Voort, L., McIntosh, S. W., et al. 2014b, Science, 346, 1255732
Edwin, P. M., & Roberts, B. 1983, Sol. Phys., 88, 179
Filippov, B., Srivastava, A. K., Dwivedi, B. N., et al. 2015, MNRAS, 451, 1117
Goossens, M., Andries, J., Soler, R., et al. 2012, ApJ, 753, 111
Heyvaerts, J., & Priest, E. R. 1983, A&A, 117, 220
Iijima, H., & Yokoyama, T. 2017, ApJ, 848, 38
Jess, D. B., Mathioudakis, M., Erdélyi, R., et al. 2009, Science, 323, 1582
Kohutova, P., Verwichte, E., & Froment, C. 2019, A&A, 630, A123
Lemen, J. R., Title, A. M., Akin, D. J., et al. 2012, Sol. Phys., 275, 17
Luo, Q. Y., Wei, F. S., & Feng, X. S. 2002, A&A, 395, 669
Mackay, D. H., Karpen, J. T., Ballester, J. L., Schmieder, B., & Aulanier, G. 2010, Space Sci. Rev., 151, 333
Nakariakov, V. M., & Verwichte, E. 2005, Liv. Rev. Sol. Phys., 2, 3
Pariat, E., Antiochos, S. K., & DeVore, C. R. 2009, ApJ, 691, 61
Schad, T. A. 2018, ApJ, 865, 31
Schmieder, B., Guo, Y., Moreno-Insertis, F., et al. 2013, A&A, 559, A1
Shelyag, S., Keys, P., Mathioudakis, M., & Keenan, F. P. 2011, A&A, 526, A5
Shetye, J., Verwichte, E., Stangalini, M., et al. 2019, ApJ, 881, 83
Shibata, K., & Uchida, Y. 1986, Sol. Phys., 103, 299
Soler, R., Terradas, J., Oliver, R., & Ballester, J. L. 2019, ApJ, 871, 3
Srivastava, A. K., Shetye, J., Murawski, K., et al. 2017, Sci. Rep., 7, 43147
Török, T., Aulanier, G., Schmieder, B., Reeves, K. K., & Golub, L. 2009, ApJ, 704, 485
Van Doorsselaere, T., Nakariakov, V. M., & Verwichte, E. 2008, ApJ, 676, L73
Velli, M., & Liewer, P. 1999, Space Sci. Rev., 87, 339
Wedemeyer-Böhm, S., Scullion, E., Steiner, O., et al. 2012, Nature, 486, 505
Xue, Z., Yan, X., Cheng, X., et al. 2016, Nat. Commun., 7, 11837